LANGMUIR

Article

pubs.acs.org/Langmuir

Microfluidic SAXS Study of Lamellar and Multilamellar Vesicle Phases of Linear Sodium Alkylbenzenesulfonate Surfactant with Intrinsic Isomeric Distribution

Andreas S. Poulos,*[,†] Manuela Nania,[†] Paul Lapham,[§] Ruhina M. Miller,[†,‡] Andrew J. Smith,[∥] Hossam Tantawy,[§] Joel Caragay,[§] Jérémie Gummel,[§] Oscar Ces,[‡] Eric S. J. Robles,[§] and João T. Cabral*[,†]

[†]Department of Chemical Engineering and [‡]Department of Chemistry and Institute of Chemical Biology, Imperial College London, London SW7 2AZ, United Kingdom

[§]The Procter & Gamble Company, Newcastle Innovation Centre, Newcastle-Upon-Tyne NE12 9TS, United Kingdom

[∥]Diamond Light Source, Harwell Science and Innovation Campus, Didcot OX11 0QX, United Kingdom

ABSTRACT: The structure and flow behavior of a concentrated aqueous solution (45 wt %) of the ubiquitous linear sodium alkylbenzenesulfonate (NaLAS) surfactant is investigated by microfluidic small-angle X-ray scattering (SAXS) at 70 °C. NaLAS is an intrinsically complex mixture of over 20 surfactant molecules, presenting coexisting micellar (L_1) and lamellar (L_α) phases. Novel microfluidic devices were fabricated to ensure pressure and thermal resistance, ability to handle viscous fluids, and low SAXS background. Polarized light optical microscopy showed that the NaLAS solution exhibits wall slip in microchannels, with velocity profiles approaching plug flow. Microfluidic SAXS demonstrated the structural spatial heterogeneity of the system with a characteristic length scale of 50 nL. Using a statistical flow−SAXS analysis, we identified the micellar phase and multiple coexisting lamellar phases with a continuous distribution of *d* spacings between 37.5 and 39.5 Å. Additionally, we showed that the orientation of NaLAS lamellar phases is strongly affected by a single microfluidic constriction. The bilayers align parallel to the velocity field upon entering a constriction and perpendicular to it upon exiting. On the other hand, multilamellar vesicle phases are not affected under the same flow conditions. Our results demonstrate that despite the compositional complexity inherent to NaLAS, microfluidic SAXS can rigorously elucidate its structure and flow response.

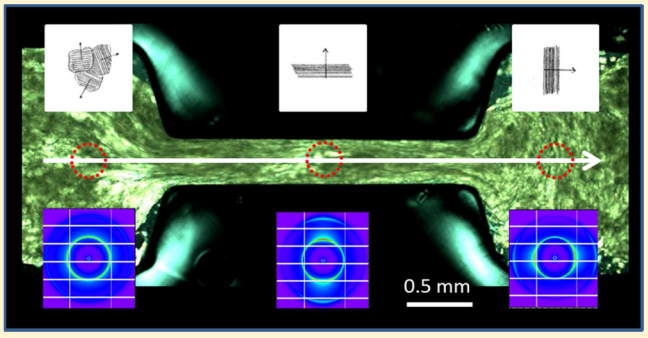

1. INTRODUCTION

A characteristic feature of soft materials is that weak external perturbations such as flow can produce drastic structural changes. These, in turn, determine macroscopic material properties, including optical and rheological.[2] The interplay between an imposed flow field of specific type and magnitude and the microstructure and rheological behavior of complex fluids remains a subject of intense fundamental research[3−7] with profound technological applications.

Surfactant solutions, employed in many everyday products such as detergents, shampoos, fabric softener, paints, pharmaceuticals, and foods,[8] are a typical example of materials where flow behavior plays a major role in their manufacture as well as in their use. At elevated concentrations surfactant solutions may form lyotropic liquid-crystalline phases due to self-assembly.[9] The mesoscopic structure of these ordered phases is anisotropic in the nanometer range, but they still retain flowability albeit with rather complex rheological behavior.[10−12] Small-angle X-ray and neutron scattering (SAXS/SANS) are the most appropriate experimental techniques for the noninvasive structural study of liquid-crystalline phases,[13] while cryo-preparation techniques are generally required for high-resolution microscopy.[14,15]

One of the most common mesophases is the lamellar (L_α) phase which is composed of a regular array of fluid surfactant bilayers separated by solvent. Lamellar phases are characterized by the spacing between bilayers *d* and the director **n** which is normal to the bilayers. Shear-induced structure and shear-induced transitions of lamellar phases have been reported for over two decades, generally in simple flow geometries.[16−20] Under shear the bilayers can align in three principal directions; the *a*, *b*, and *c* orientations have the director parallel to the neutral, velocity, and velocity-gradient directions, respectively.[17,21] Under certain conditions the bilayers can sufficiently bend and wrap around each other forming multilamellar vesicles (MLVs), whose overall diameters can range from tens of nanometers to microns.[22−27] The flow regimes that correspond to different orientations and the MLV transition have been mapped in "dynamic phase diagrams" for model surfactant mixtures containing anionic sodium dodecyl sulfate (SDS)[16] and nonionic surfactants[26,28−30] almost exclusively under simple

Received: April 1, 2016
Revised: May 17, 2016
Published: May 19, 2016

DOI: 10.1021/acs.langmuir.6b01240
Langmuir 2016, 32, 5852−5861

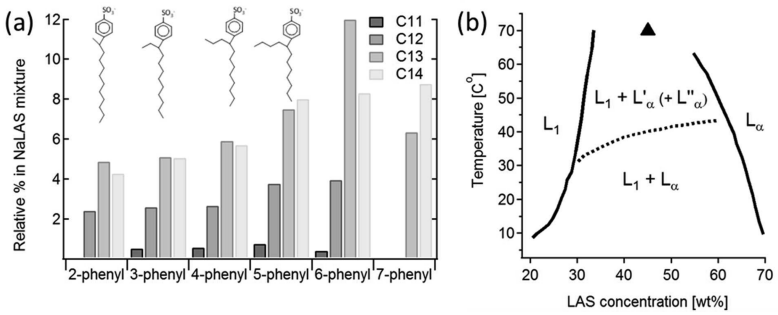

Figure 1. (a) Relative abundance of NaLAS surfactant phenyl positional isomers in a typical industrial mixture containing homologues with different alkyl chain lengths (C_{11} to C_{14}) and phenyl positional isomers (2- to 7-phenyl). The chemical structure of the 2- to 5-phenyl isomers of NaLAS with a C_{12} chain is shown above the bar chart. (b) Adapted phase diagram of the NaLAS−water system,[1] showing a wide two-phase region at intermediate NaLAS concentrations composed of a micellar phase (L_1) and a lamellar L_α liquid crystalline phase. The horizontal line separates optically opaque two-phase samples from translucent samples at higher temperatures where lateral phase separation has been observed, indicative of two lamellar phases L'_α and L''_α in addition to L_1. The system studied is marked with a triangle.

shear. On the other hand, industrially relevant surfactant systems are more complex because of inherent polydispersity of the molecule itself, mixture of surfactants, or because of the presence of additives such as polymers, electrolytes, etc., necessary for each specific application.

Here we concentrate on the phase and flow behavior of linear sodium alkylbenzenesulfonate (NaLAS), one of the most widely used anionic surfactants in the world. NaLAS consists of an alkyl chain grafted to a benzene ring with a sulfonate group responsible for its detergency. NaLAS synthesis results in alkyl chains of different lengths (from C_{11}−C_{14}) and a series of phenyl isomers where the benzene group can be grafted to the 2, 3, 4, 5, 6 and 7-positions in the alkyl chain, illustrated in Figure 1a. This yields a fairly heterogeneous system where the 2−3 phenyl isomers can be considered linear surfactants and the 5−7 phenyl isomers as having two short tails. During detergent manufacture, NaLAS is normally diluted in water leading to the formation of multiple micellar and lamellar phases, whose structure has an impact on the properties of the final product. Specifically, a transition from planar NaLAS lamellar bilayers to MLVs has been found to yield a "firmer and less adhesive" paste with enhanced "stability".[31] In general, surfactant microstructure, coexistence of multiple lamellar phases, and MLV size distribution are known to profoundly affect rheological response, impacting powder detergent manufacture, stability, dissolution profile, and powder flow properties.[31,32] Approximate phase diagrams have been published both for the individual NaLAS isomers[33,34] and also for an industrial NaLAS mixture similar to the one used here (Figure 1b).[1,35] At intermediate NaLAS concentrations at ∼25 °C (30%−70%) there is a wide domain where an L_1 (micellar) phase coexists with an L_α (lamellar) phase. As a consequence of the natural variability in the chemical structure of NaLAS, the micellar phase is richer in the NaLAS 2−3 isomers, whereas the lamellar phase richer in the 5−7 isomers.

Another striking property of the NaLAS−water system is the appearance of multiple coexisting lamellar phases with different *d* spacings. This lateral phase separation has been observed in many previous studies[35] (with an exception where only a broad SAXS peak was observed[1]), even in those which used single NaLAS isomers[33,34] and thus cannot be due to surfactant polydispersity. A short to medium range attraction between bilayers probably of electrostatic origin has been invoked to explain lateral phase separation, but direct evidence is still lacking.[34] The structure of the coexisting lamellar phases is also unclear. Most evidence points to the formation by diffusion of 10−100 nm domains of different composition within the fluid bilayers[36] (similar to lipid rafts[37]). The domains are correlated across many lamellae (at least 20 to give sharp SAXS peaks) and thus give different *d* spacings.

It is also well-known that the addition of electrolytes has a large effect on the phase behavior of NaLAS.[36] It promotes lateral phase separation and also the transformation of lamellar sheets to MLVs. Although the two phases are thermodynamically identical, they exhibit markedly different rheological properties which are critical in designing and optimizing the manufacturing process.[38] Hence, understanding the microstructure and mechanism of their response to flow is critical for improving the formulation of NaLAS-based products.

Here, we use microfluidics coupled to polarized light optical microscopy and synchrotron SAXS to investigate the structure of NaLAS/water mixtures under flow. The combination of microfluidics with small-angle scattering has recently been proven invaluable in the study of flow-induced structure in model systems.[4,5,39,40] We focus on contraction−expansion flow imposed by a single constriction, thus forcing the fluid to accelerate and decelerate in a controlled way. The actual microfluidic device used and a schematic of this geometry are shown in Figures 2a and 2b, along with the geometrical prediction of the fluid velocity and acceleration along the centerline of the channel assuming a Newtonian fluid (Figure 2c). This type of flow was chosen because it is predominantly extensional and it provides insight into important processes such as fluid injection where fluids are forced through small orifices.

The paper is structured as follows. First, we establish by optical microscopy the flow behavior of the binary NaLAS−water system at 45% concentration and high temperatures ($T = 70$ °C), subject to constriction flow. Employing synchrotron SAXS, we carry out statistical analysis of the distribution of lamellae spacings in this compositionally heterogeneous system. We then determine the structure of the coexisting micellar and lamellar phases and show that by deconvoluting their respective signals their relative abundance can be quantified. Furthermore, we examine the effect of flow through a microfluidic constriction on the structure and orientation of the lamellar sheets and compare that to the MLVs. Finally, we produce a full map of 200 × 400 μm mesh size of the bilayer orientation through a constriction and compare that to the flow field obtained by optical microscopy.

DOI: 10.1021/acs.langmuir.6b01240
Langmuir 2016, 32, 5852−5861

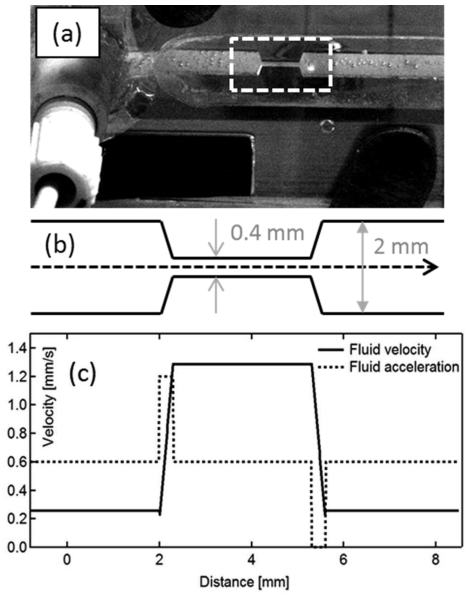

Figure 2. (a) Microfluidic chip mounted on the SAXS beamline. The flow connector is visible at the bottom left corner. Note the drilled elliptical hole around the channel. (b) Schematic of microfluidic chip design: 2 mm wide channel with a single constriction of 0.4 mm width and constant channel thickness of 0.54 mm. The flow direction is from left to right with a typical flow rate of 1 mL/h. (c) Average fluid velocity and acceleration along the centerline of the channel based on a flow rate of 1 mL/h assuming plug flow.

2. MATERIALS AND METHODS

NaLAS Samples. Linear sodium alkylbenzenesulfonate was obtained from Procter & Gamble Newcastle Innovation Centre and used as received. At the surfactant concentration of 45% and room temperature the material was heterogeneous, as expected. Immediately before the microfluidic SAXS or optical microscopy experiments, the material was heated to 70 °C and vigorously shaken. The resulting white paste was used to fill syringes, maintained at 70 °C throughout the experiments, which were then transferred to the beamline or microscope. At temperature of the actual experiment ($T \sim 70$ °C), the material becomes less opaque and slightly translucent. The lamellar sheets were transformed to multilamellar vesicles (MLVs) by slow addition of Na_2SO_4 (Sigma-Aldrich) while stirring the NaLAS paste with an overhead mixer at 70 °C. The addition of sodium sulfate decreases the nominal surfactant concentration to 33%.

Microchip Preparation and Experimental Setup for High *T* SAXS Experiments. Devices were fabricated by single step frontal photopolymerization (FPP) of a thiol−ene copolymer (NOA 81, Norland Adhesives) within thin borosilicate plates (150 μm) of 24 × 50 mm size with appropriate spacers that determine the thickness of the channels, following previously published procedures.[5] For the SAXS experiments, the spacers were 540 μm thick, defining the microchannel depth. The microchip was mechanically reinforced with a thicker glass plate (t = 1.1 mm) with a diamond-drilled central slit over the region of interest that allowed X-ray scattering experiments to be performed with reasonable transmission corresponding to a total thickness ≈300 μm of borosilicate glass. The reinforcement imparts rigidity, enabling easy handling, mounting, port connection, and operation. The device was mounted on a temperature-controlled aluminum frame and pedestal with a slit aligned with the microchannels and the beam path. The aluminum frame was mounted perpendicularly to the X-ray beam and heated to 70 °C by two electrical heaters connected to a temperature controller (CAL 3300, Cal Controls).

Disposable 20 mL syringes were filled with sample at a temperature of 70 °C and wrapped in flexible syringe heater pads (Braintree Scientific, BS-SYR). The syringes were attached to a syringe pump (Braintree Scientific, BS-8000), remotely controlled via an RS232 cable and a computer with a custom-made LabVIEW program (National Instruments). The syringes were connected to PEEK tubing (Sigma-Aldrich, o.d. 1/16 in., i.d. 0.03 in.) via Luer lock barb adapters (Cole-Parmer). The tubing was wrapped in aluminum foil, and its length was kept to a minimum ($L \approx 40$ cm) to avoid excessive heat losses between the syringe and the microchip. The tubing was then connected to the chip via an attached nanoport (N-333 NanoPort, 10-32 Coned, IDEX Health & Science). Each microchip was typically used between 2 and 4 h of continuous operation.

Optical Microscopy. Optical birefringence texture images were obtained with an Allied Vision Manta G-235C digital camera working at 45 Hz mounted on an IX71 Olympus inverted transmission microscope with a 5× Olympus objective lens. Image analysis was performed postacquisition using the ImageJ open source analysis software. In order to calculate the displacement field between images, we used the open source JPIV software program for particle image velocimetry.

SAXS and Beamline Configurations. The results presented here were obtained in two separate synchrotron runs at the I22 beamline, Diamond Light Source. In the first run, a photon energy of 12.4 keV was used (λ = 0.1 nm); the sample−detector distance was measured using an AgBe capillary and was 1.53 m. In the second run, a photon energy of 17 keV was used (λ = 0.73 nm). The sample-to-detector distance was 2.28 m. Simultaneous SAXS and WAXS patterns were acquired. The SAXS data were reduced and analyzed with the Nika package running on Igor Pro (J. Ilavsky, Argonne National Laboratory[41]). One should also note that scattering gives structural information only in the real-space directions perpendicular to the beam. The third spatial direction parallel to the beam is not accessible, so all the results presented here necessarily are applicable to the two accessible directions: one parallel to the flow direction and one perpendicular.

3. RESULTS AND DISCUSSION

Flow Behavior of 45% NaLAS−Water. The 45% NaLAS−water mixture is a two-phase system and exhibits rather complex flow behavior. Figure 3a shows polarized light optical microscopy textures of a 45% NaLAS−water sample flowing through a constriction at 70 °C and volumetric flow rate Q = 1 mL/h. The lamellar (L_α) phase is weakly birefringent, but it does not present the characteristic textures of focal conics and oily streaks,[42] likely due to the high sample opacity, yellowish color, and relatively large optical path (0.54 mm) of the microfluidic device. Close to the walls of the wide channels we can detect the isotropic nonbirefringent micellar (L_1) phase. This is especially evident in the corners of the constriction, but it is also present in the straight inlet and outlet channels in a thin layer of 50−200 μm.

The flow field can be computed by digital image correlation by following the variations in birefringence intensity. The relative displacements of the fluid between successive images are shown in Figure 3b. As expected, the presence of the narrow channel perturbs the flow. It converges and accelerates as it enters the constriction and diverges in a fan-shaped pattern and decelerates as it exits the constriction. Moreover, in the wide channels both before and after the constriction the velocity is constant along the width of the channel and goes rapidly to zero only in the vicinity of the walls. This plug flow velocity profile in the wide channels can be explained by the presence of the thin layer of micellar L_1 phase next to the walls. This low-viscosity phase lubricates the flow of the lamellar phase which due to its high viscosity and elasticity maintains its shape as it flows downstream, effectively behaving like a viscoelastic solid. An important consequence of this type of flow field is that the fluid is experiencing no shear strain in the wide channels both before and after the constriction. At the same time, it is experiencing a considerable amount of extensional strain that can be estimated as follows. Assuming plug flow, a nominal flow rate Q will give a uniform fluid velocity $v_0 = Q/(w \times t)$. In the narrow channel the fluid velocity will

DOI: 10.1021/acs.langmuir.6b01240
Langmuir 2016, 32, 5852−5861

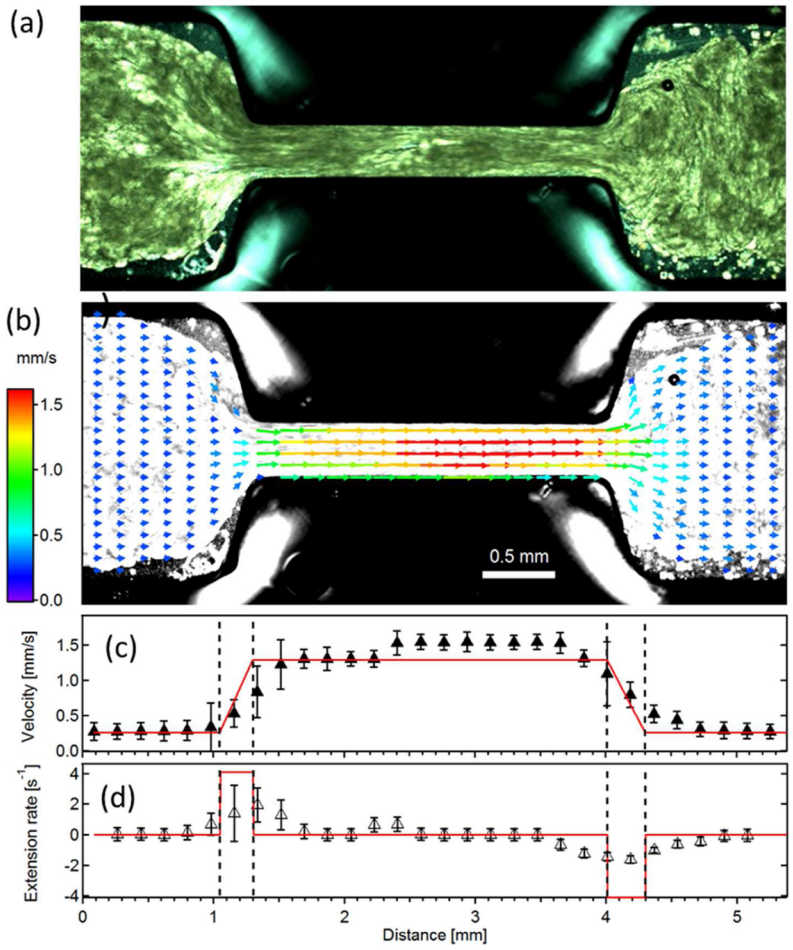

Figure 3. (a) Polarized optical microscopy image of a 45% NaLAS−water system flowing through a constriction at a flow rate of 1 mL/h. (b) Flow field of the same sample obtained by digital image correlation and averaging of 30 successive images. (c) Fluid velocity as a function of horizontal position along the centerline of the channel. The red line indicates the velocity prediction based on the channel geometry and assuming plug flow of a Newtonian fluid. The dashed vertical lines indicate the positions of the entrance and exit of the constriction. (d) Extensional rate as a function of horizontal position along the centerline of the channel. The red line indicates the extensional rate prediction assuming the previous velocity profile.

increase to $v_{max} = (20/4)v_0$. The extension rate $\dot{\epsilon}$ along the centerline can then be calculated as the change in fluid velocity over the length of the constriction entrance or exit: $\dot{\epsilon} = \Delta v/\Delta L$.

The measured and predicted velocities along the centerline of the channel are shown in Figure 3c. When the channel starts to narrow, the velocity increases linearly with distance to approximately 5 times its original value, consistent with a reduction of the channel width by 4/5. Further down the constriction the velocity increases slightly, and then at the constriction exit it decreases to its initial value. However, the velocity change upon entering and exiting the constriction happens over a longer distance of 0.6 ± 0.2 mm compared to the predicted distance of 0.3 mm based on the geometry of the channels. This has a large effect on the measured extensional rates which are shown in Figure 3d and attain at maximum half the value predicted by the geometry of the constriction. This discrepancy shows that the rheological behavior of the fluid evidently affects the flow behavior. For a highly elastic fluid such as an L_α phase[43] it is expected that an imposed perturbation in the flow field (e.g., a constriction) will propagate both upstream and downstream. Hence, knowledge of the channel geometry is not enough to predict the flow field which in practice should always be experimentally determined.

The velocity profiles perpendicular to the flow direction can be seen in Figure 4 at three horizontal positions: before, in the middle, and after the constriction. It is clear that in the wide channels the flow is pluglike. On the other hand, all along the constriction the velocity profile becomes approximately parabolic with nonzero velocity at the walls and a calculated slip

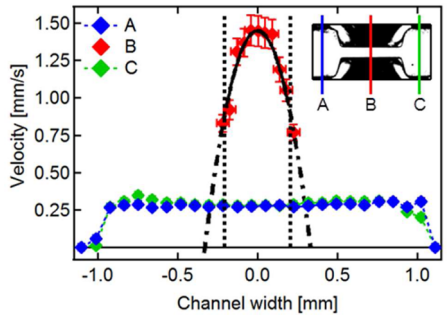

Figure 4. Velocity profiles of 45% NaLAS−water system flowing through a constriction at a flow rate of 1 mL/h. It can be seen that before and after the constriction the lamellar phase flows in plug flow, whereas in the middle of the constriction it has a parabolic velocity profile with a slip length L_s = 0.13 mm.

DOI: 10.1021/acs.langmuir.6b01240
Langmuir 2016, 32, 5852−5861

length L_s = 0.13 mm. We believe that this change of velocity profile comes from the converging flow at the entrance of the constriction and the increased flow rate; both promote mixing of the L_α and L_1 phases into a more uniform fluid that will interact with the walls of the channel. The increased uniformity of the fluid can be also seen in Figure 3a where in the narrow channel we can no longer distinguish a separate L_1 phase close to the walls. This might also explain the slight velocity increase in the second half of the constriction as the progressive change of the velocity profile from plug flow to parabolic leads to a maximum velocity higher than the average velocity and not identical. Of course, it can also be due to a small variation in the height of the channels.

Structure of 45% NaLAS−Water System under Flow. Optical microscopy has allowed us to establish the flow field of the 45% NaLAS−water system as it passes through a constriction. To relate that to changes in the microstructure, we have obtained small-angle X-ray scattering (SAXS) patterns throughout the microfluidic device under identical conditions. The curve shown in red in Figure 5a is a typical SAXS curve of a

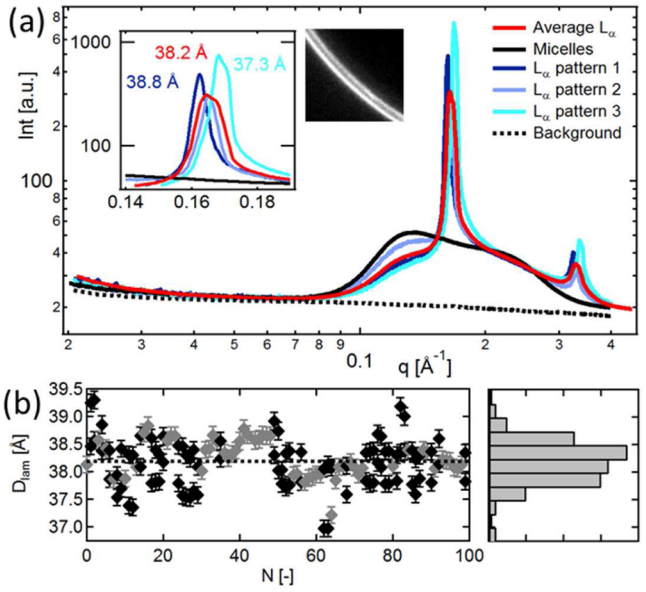

Figure 5. (a) SAXS patterns of three individual 1 s frames (blue lines) compared to the average of 100 frames (red line). The SAXS pattern of the micelles (black line) and the background scattering of the empty channel (black dashed line) are shown for comparison. Inset: zoom around the L_α peak shows the presence of multiple lamellar peaks and the variability in d. (b) d vs frame number for 100 SAXS patterns at the same spot on the chip. The gray points correspond to frames where only one peak is present and the black points to frames where multiple peaks are present. The average d = 38.2 Å is shown with a dashed horizontal line. A histogram of the values is shown on the right.

long acquisition (100 s) in the wide inlet channel before the constriction at a volumetric flow rate Q = 1 mL/h. The two relatively sharp quasi-Bragg peaks at 1:2 q ratios along with the absence of any WAXS peaks (data not shown) suggests the presence of an L_α phase with a lamellar spacing d of 38.2 Å.[13,44] At the same time a very broad background peak is visible at 0.09−0.13 Å^{-1}. This is due to the micellar phase that is always present in the 45% NaLAS−water system. In the wide inlet channel all SAXS patterns show no or small anisotropy. Hence, although the material is under flow, the absence of shear due to plug flow impedes the expected alignment of the bilayers in one of the favored orientations.

As we have already seen the material appears quite heterogeneous in optical microscopy. Hence, the local structure can differ considerably from the average structure established from long SAXS acquisitions. To study this heterogeneity, we compare in Figure 5a three individual 1 s SAXS patterns (blue lines) to the average pattern. Given the dimensions of the channels and the flow velocity shown in Figure 3b, a single 1 s SAXS pattern corresponds to a scattering volume of 50 nL. Compared to the average pattern, individual frames show great variability in the main lamellar peak position and shape and the intensity of the broad micellar scattering signal. The main peak of individual frames is also often asymmetric and contains subsidiary peaks that correspond to different d (inset of Figure 5a). The 2D scattering pattern in Figure 5a shows an example of such clearly resolvable peaks with two specific d's that should correspond to lamellar domains with different compositions. In Figure 5b, d is plotted as a function of frame number for 100 frames, with gray points corresponding to frames with single peaks and black points to frames with multiple peaks. The spacing varies irregularly from frame to frame between 37 and 39.5 Å. A histogram of d shows a continuous distribution of values around the mean and not specific d's which are more prevalent. All of the above suggest that the heterogeneity of the material at the 50 nL scale comes from coexisting L_α phases with different d between 37 and 39.5 Å, but always in the presence of a significant fraction of micelles.

While the isomeric distribution is generally associated with lateral phase separation, the continuous d-spacing distribution within the scattering volume probed indicates that such heterogeneity has a characteristic volume below 50 nL. Micro/nano-focused X-ray beam scanning experiments might be able to increase our spatial resolution and establish correlations with a finer mesh. We can also compare the different lamellar spacings to the size of NaLAS isomers. The difference in length of a 6-phenyl NaLAS isomer from a 2-phenyl isomer is approximately 3 Å, assuming a fully stretched C_{12} chain giving a 6 Å difference in bilayer thickness. Assuming that all else is equal this would translate to a similar difference in d—more than double of what we observe. This simple calculation implies that the bilayers in a single lamellar domain are composed of different isomers so that the maximum observed changes in lamellar spacing are not as extreme as those suggested by the size of the molecules.

In Figure 6 we show in more detail that the total scattered intensity can be decomposed into three contributions: the background (gray), the micelles (blue), and the L_α phases (red), so that the total intensity can be written as $I(q) = I_{back}(q) + f_{mic}I_{mic}(q) + I_{lam}(q)$. The micellar contribution depends on the fraction of micelles f_{mic} that are contained in the scattering volume during the acquisition. As we have seen in Figure 3a, the micellar phase can be predominantly found close to the walls of the channel. Thus, a SAXS pattern anywhere along the wall will contain scattering from the micellar solution that coexists with the lamellar phases in the 45% NaLAS−water system. This is shown in Figures 5a and 6a (black line) and is characteristic of strongly interacting micelles. The scattered intensity of the micelles starts to increase above the background at q = 0.09 Å^{-1} and presents a broad peak at q = 0.13 Å^{-1}. In this range of scattering vectors the signal from the L_α phases is negligible, and hence the scattered intensity can be used to estimate the fraction of micelles f_{mic} present in the scattering volume. In the inset of Figure 6a we show f_{mic} as a function of frame number. It attains

DOI: 10.1021/acs.langmuir.6b01240
Langmuir 2016, 32, 5852−5861

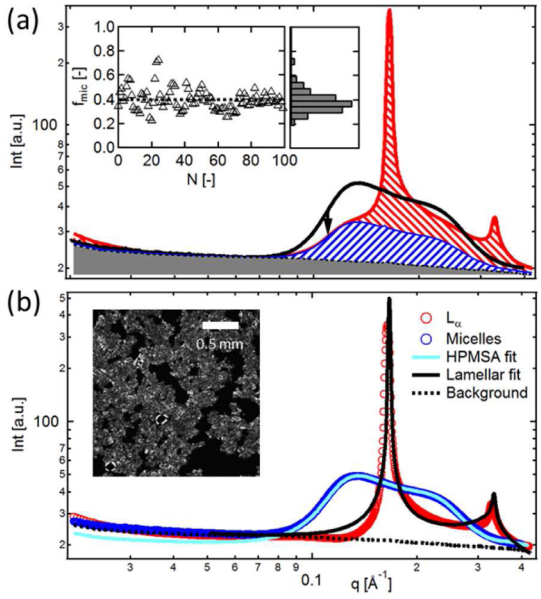

Figure 6. (a) Deconvolution of the average SAXS pattern into background (gray), micellar (blue), and pure lamellar (red) contributions. The SAXS pattern of the micelles (black line) is shown for comparison. The black arrow indicates the q value where the fraction of micelles f_{mic} is estimated. Inset: micellar fraction vs frame number for 100 SAXS patterns with an average value of 0.39 (dashed black line). The histogram is shown on the right. (b) SAXS patterns of the pure lamellar phase (red circles) and the micelles (dark blue circles). The light blue and black lines are fits to the micellar and lamellar scattering patterns, respectively. Inset: polarized light optical microscopy image of a thin layer showing isotropic micellar and birefringent L_α regions.

values between 0.2 and 0.7 with an average of 0.39 and shows a lot of variability exactly like the variability in lamellar spacings. The average fraction of micelles is also consistent with that measured by polarized light optical microscopy of very thin (~20 μm) samples. The fraction of isotropic phase present in the image shown in the inset of Figure 6b is between 0.3 and 0.4. The micellar signal is present in all SAXS patterns because the micellar phase in all probability will also be present close to the top and bottom walls of the channel that are perpendicular to the X-ray beam.

The decomposed SAXS patterns of the pure micellar phase and the lamellar phases can be seen in Figure 6b. The micelle scattering pattern can be fitted with a core−shell form factor model with a Hayter and Penfold mean spherical approximation (HPMSA) structure factor appropriate for screened electrostatic repulsions.[45,46] The fit shown in Figure 6b (light blue line) corresponds to a core radius of 14.5 Å, a shell thickness of 1.5 Å, and 0.2 overall polydispersity. The high polydispersity might also mean that the micelles are not exactly spherical, but the degree of anisotropy should be low and for certain less than two. Crucially, the electron density of the shell has to be higher than both the core and the solvent in order to produce the deep minimum at 0.07 Å^{-1}. This is of course expected as the estimated electron density of the hydrophilic $-SO_3$ NaLAS headgroups is twice that of water. The interaction between micelles is modeled with an HPMSA structure factor for screened electrostatic repulsions which gives the broad peak at 0.13 Å^{-1}. The free HPMSA parameters used in this fit are the interaction diameter D = 41 Å, the total micellar charge of 40 e$^-$, the volume fraction ϕ = 17%, and the monovalent salt concentration of 0.34 M. The fixed parameters are the temperature (T = 70 °C) and the dielectric constant (ε = 78). The micellar volume fraction extracted from this model is 17%, which agrees rather well with simple estimates on the repartition of NaLAS between the L_α and micellar phases. Hence, the 45% NaLAS−water system consists of a ratio of 0.39/0.61 micelles to lamellar phases with respective NaLAS volume fractions of 17%/55%, giving an overall NaLAS volume fraction of 40% consistent with the nominal 45% mass fraction assuming a NaLAS density slightly higher than water.

The SAXS pattern from the pure lamellar phase can also be fitted by using a model proposed by Nallet et al. that takes into account thermal undulations of the bilayers.[44] The fit is shown in Figure 6b (black line) and is less satisfactory than that of the micellar signal. Of course, as we have seen before, the SAXS pattern actually comes from coexisting lamellar phases with different d so it does not exactly correspond to the model. Nevertheless, some interesting parameters can be extracted with relative confidence. The electron density of the bilayer is about 2.5 times higher in the headgroup region than in the tails. The bilayer total thickness is between 18 and 22 Å, with a headgroup thickness of 0.5−2 Å. This translates to a 48−58% surfactant volume fraction in a typical bilayer.

Constriction-Induced Reorientation. SAXS patterns were acquired along the channel centerline to determine the microstructure as the fluid is accelerated and decelerated through the extensional flow. By measuring the transmission of the X-ray beam in small steps in the horizontal and vertical directions (xy), a map of the chip geometry is obtained (Figure 7a) to enable accurate positioning of the beam with respect to the constriction. The 2D SAXS patterns at three representative points along the centerline of the channel are shown in Figure 7b. At the wide inlet channel (Figure 7b, position A) just before any acceleration of the fluid, the 2D SAXS pattern is isotropic with two orders of reflection visible. In the middle of the constriction (Figure 7b, position B), the SAXS pattern changes significantly: it is strongly anisotropic with high intensity in the vertical direction and much lower intensity in the horizontal (flow) direction, indicating that in the constriction the bilayers are preferentially aligned parallel to the flow direction. When the fluid exits the constriction (Figure 7b, position C), the SAXS pattern again shows strong anisotropy, but this time the intensity is highest in the horizontal (flow) direction. This indicates that the fluid deceleration has forced most bilayers to rotate by 90° and preferentially align perpendicularly to the flow direction. This rotation happens over a distance of approximately 0.4 mm as discussed below. Reorientation of bilayers perpendicular to the flow direction has been previously reported for the lamellar phases of CTAC/pentanol/D_2O and SDS/octanol/brine systems,[5,39] and for cylindrical micelles,[47] and thus appears to be a general feature of anisotropic and disklike objects. As this behavior is not specific to the NaLAS lamellar phase, we do not interpret it in the context of its isomeric distribution or lateral phase separation. Instead, it is most probably a direct consequence of the flow field. Upon exiting the constriction, the fluid experiences an extensional flow field normal to the flow direction which reorients the sheets similar to the reorientation mechanism of cylindrical micelles.[47]

The radial $I(q)$ and azimuthal $I(\phi)$ profiles of the scattered intensity can be seen in Figures 7c and 7d, respectively. It is clear that $I(q)$ does not appreciably change as the fluid moves through the constriction. The lamellar periodicity remains the same, and no change is observed in the intensity of reflections (or the intensity at very small-angles) which would indicate a change of microstructure at nanometer length scales or the formation of multilamellar vesicles (MLVs). On the other hand, the azimuthal

DOI: 10.1021/acs.langmuir.6b01240
Langmuir 2016, 32, 5852−5861

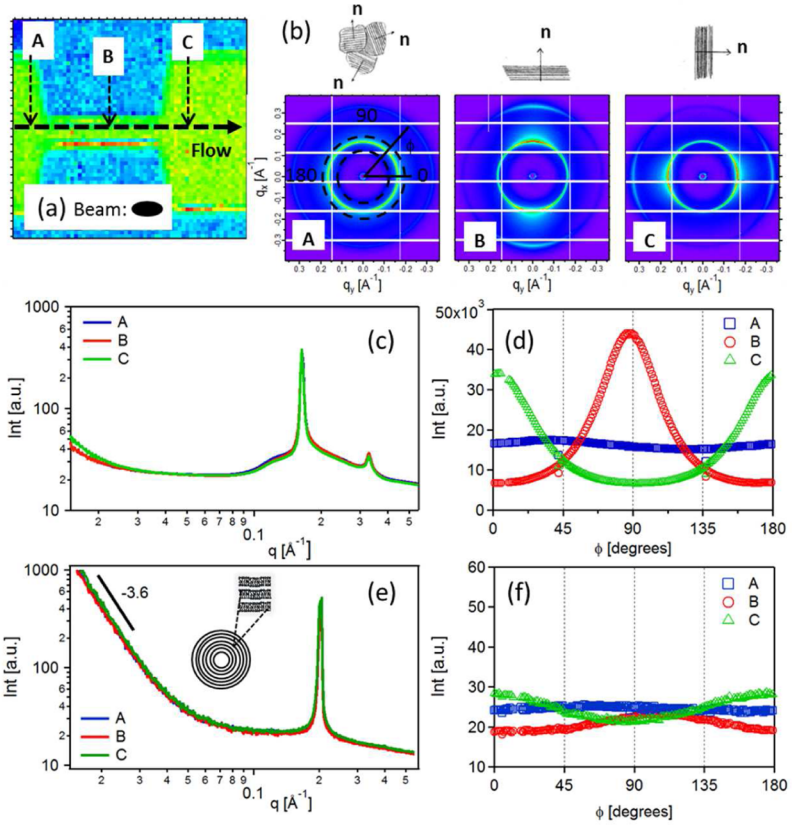

Figure 7. Effect of contraction−expansion flow on of 45% NaLAS−water system at 70 °C. (a) X-ray transmission map of the chip, showing clearly the position of the channel. The X-ray beam size and shape is shown to scale. (b) 2D SAXS patterns at three representative positions along the centerline of the microchannel. The angle ϕ and range of integration are shown in the first 2D pattern. (c) Radial profile of the intensity $I(q)$ at positions A, B, and C ($\Delta q = 3.25 \times 10^{-4}$ Å^{-1}). (d) Azimuthal profile of main peak intensity $I(\phi)$ at positions A, B, and C ($\Delta\phi = 0.5°$). (e) (f) Radial and azimuthal intensity profiles of the MLV forming system at positions A, B, and C.

profiles show considerable change. Before the constriction the profile is flat, indicating isotropic scattering and a powder pattern. In the constriction the intensity shows a strong peak at around ϕ = 90°, indicating that the bilayers align parallel to the wall of the channel. Just after the constriction, the peak shifts to 0°, indicating a rotation of the bilayers perpendicular to the flow direction.

By diluting the 45% NaLAS−water system with electrolytes, one can promote the transformation of the micelles into lamellar liquid crystals and the lamellar sheets into MLV's. MLVs are spherical entities that contain 100s of concentric bilayers (inset schematic in Figure 7e). In Figures 7e and 7f, the radial $I(q)$ and azimuthal $I(\phi)$ profiles for the MLV forming system can be seen. In contrast to the previous lamellar SAXS patterns, only one peak is visible, and there is considerable increase in scattered intensity as $q \rightarrow 0$, indicating the presence of multilamellar vesicles (MLVs). Their uniform size in the micron range produces the extra scattering at angles considerably lower than the bilayer correlation peak which is at nanometer length scales, and the presence of curvature decreases the degree of order in the system suppressing the second peak at q_{002}.[16] Moreover, the broad micellar signal is absent as all the micelles are transformed into the lamellar phase. The significant decrease in d-spacing is due to the salting-out effect and not due to crystallization (no peak in WAXS).

It is clear that the radial profile of the intensity does not change as the material passes through the constriction. At the same time, the azimuthal profile of the peak intensity shows only weak anisotropy, with the bilayers oriented parallel to the flow direction in the constriction and perpendicular to it at the exit. To compare the alignment of the two systems, we can estimate the anisotropy by taking the ratio of the peak-to-trough value of the intensity with the maximum value: $A = (I_{\phi,\max} - I_{\phi,\min})/I_{\phi,\max}$. The parameter A can take values between 0 and 1 for no anisotropy and maximum anisotropy, respectively. For the L_α sheets, A is 0.13, 0.85, and 0.80 at positions A, B, and C, respectively (Figure 7d). On the other hand, for the MLVs (Figure 7f), the respective values of A are 0.05, 0.19, and 0.24 reflecting the much lower overall anisotropy of the structure.

Our results have shown that MLVs are relatively insensitive to contraction−expansion flows whereas lamellar sheets show strong orientation. This effect correlates with the better manufacturability of MLVs, as fluids with a lamellar sheet structure experience changes under flow which generally translate into rheological changes. It is well-known that the rheological properties of a lamellar phase depend on orientation.[43] Hence, any kind of flow field (such as extensional flow) that is encountered during processing will orient them to some degree and change their rheology. On the other hand, MLV's will retain their structure, and hence one might expect that their rheological properties are independent of their past processing history.

In previous studies of L_α phases under elongational flow, the lamellar spacing d was seen to decrease by a maximum of 5% for extension rates $\dot{\epsilon} \geq 0.3$ s^{-1}.[48,49] This was attributed to the suppression of undulations due to the flow field which led to

DOI: 10.1021/acs.langmuir.6b01240
Langmuir 2016, 32, 5852−5861

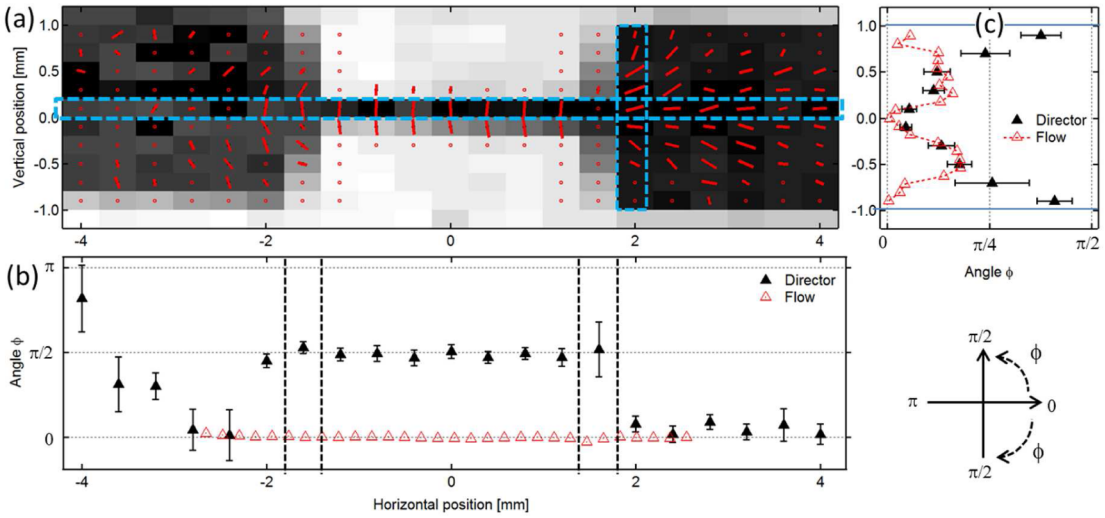

Figure 8. (a) Combined transmission and L_α phase director orientation map with a 0.2 mm (V) × 0.4 mm (H) mesh size of a 45% NaLAS−water sample flowing from left to right at a flow rate of 1 mL/h. The investigated area on the chip has dimensions of 2.2 mm (V) by 8 mm (H) around a single constriction. The transmission of each sector is given in grayscale. The length of each vector represents the anisotropy A of the SAXS pattern (as described in the text), and the direction of the vector represents the orientation of the bilayer normal. (b, c) Horizontal and vertical cuts through the orientation map: comparison of the inclination of the lamellar phase director and the flow direction extracted from the optical microscopy data of Figure 3b.

stretching and straightening of the lamellae, a decrease in bilayer excess area and consequently to a decrease in spacing.[48−50] Martin et al. have observed, by contrast, a significant increase of lamellar spacing of CTAC/octanol/brine system.[39] Under the flow conditions studied here, we have not observed a change in spacing for the NaLAS−water system.

SAXS Mapping of a Microfluidic Constriction. All the results presented up to here were obtained along the centerline of the microchannel. Hence, they represent the structure and orientation of the phase as it is uniaxially accelerated and decelerated. We next consider the microstructure of a 45% NaLAS−water system flowing at 1 mL/h at all points with respect to the centerline, where the flow field is more complex.

In Figure 8a, we show the result of SAXS mapping with a 0.2 mm (V) × 0.4 mm (H) mesh size. At each position, we obtain both the transmission of the beam and the SAXS pattern. The transmission is shown as the grayscale color of each sector and readily shows the positioning of the constriction, allowing the identification of all the relevant points such as the vertical position, the entrance, and exit of the constriction. SAXS patterns are obtained at each point on the grid from the top right and are analyzed as before by extracting the radial and azimuthal profiles. Similarly to the SAXS patterns along the centerline, the radial profiles show very little variation with both horizontal and vertical position with the exception of a thin 0.2 mm layer close to the walls of the wide channels where the micellar signal dominates and the lamellar signal almost disappears. Hence, the microstructure of the material remains unaffected by the constriction. On the other hand, the azimuthal profiles show a changing degree of alignment and orientation of the bilayer normal throughout the geometry. These two parameters are captured by the vectors in Figure 8a. The length of each vector represents the degree of anisotropy $A = (I_{\phi,\max} - I_{\phi,\min})/I_{\phi,\max}$, while the direction of the vector represents the azimuthal position of the maximum and hence the average orientation of the bilayer normal.

Three observations emerge readily from the map in Figure 8a. Before the constriction the anisotropy is very low, and the orientation of the bilayers is essentially random everywhere in the channel. This indicates that flow through the wide inlet channel has no appreciable effect on the L_α phase microstructure even away from the centerline. This corroborates the conclusion from Figure 4 on the absence of shear in the channel that would in all probability align the bilayers. Second, the degree of anisotropy A stays approximately constant throughout the constriction (from −2 to 1.2 mm). Hence, under the conditions studied, the length of the constriction plays no role in the alignment effect which is only due to the extensional flow at the entrance. Finally, we note that at the exit of the constriction the orientation of the director follows a fan-shaped pattern following the flow lines. Most importantly, this fan-shaped orientation persists downstream for at least another 2 mm although the degree of anisotropy slowly decreases. The lamellar phase thus flows downstream with the bilayers aligned perpendicular to the flow direction, and the absence of shear prevents them from realigning in one of the standard orientations.

In Figure 8b,c we compare the orientation of the lamellar phase director compared to the orientation of the velocity vector, extracted from the optical microscopy data in Figure 3b. The horizontal cut in Figure 8c shows that the reorientation of the initially random lamellar phase happens at the −2 mm horizontal position even before the entrance of the constriction. The velocity vector, of course, always points along the flow direction. A vertical cut just after the exit of the constriction is shown in Figure 8c. It can be seen that close to the centerline of the chip the two angles match almost perfectly within experimental error indicating that locally and on average the bilayers are aligned always perpendicularly to the flow direction. This alignment, although counterintuitive, is a direct consequence of the deceleration of the fluid on exiting the constriction. On the other hand, further away from the centerline and close to the walls the bilayers are aligned almost parallel to the flow direction; the extensional component in the flow field far away from the centerline becomes weaker, and the bilayers are aligned by the small shear component.

DOI: 10.1021/acs.langmuir.6b01240
Langmuir 2016, 32, 5852−5861

4. CONCLUSIONS

We investigated the ubiquitous NaLAS surfactant with microfluidic SAXS, focusing on concentrated aqueous solutions at 70 °C, where micellar, lamellar, and MLV phases occur. NaLAS is currently one of the most widely used anionic surfactants in the world, and this paper seeks to elucidate, at the molecular level, the structure and response to flow of these key liquid crystalline phases. Novel microfluidic devices were fabricated in order to ensure low SAXS background, yet considerable pressure and thermal resistance, and overall robustness to handle viscous complex fluids. The devices combine the rapid prototyping advantages of photopolymerization, with mechanically reinforced substrates in closed-face lithography.

NaLAS is intrinsically a complex mixture of multiple (over 20) surfactant molecules, whose impact on structure and flow of ordered phases is unclear. Microfluidics emerges as an attractive approach for this SAXS study for two main reasons. First, controllably flowing a sample while acquiring SAXS patterns enables an unprecedented statistical analysis of the spatiotemporal variations of these complex surfactant solutions. Second, the well-defined flow fields imposed in microfluidics enable the quantitative and spatial mapping of material processing at the molecular scale.

Employing polarized light optical microscopy, we find that these concentrated surfactant solutions (45% mass fraction) exhibit considerable wall slip, with velocity profiles approaching plug flow. Our statistical flow-SAXS analysis of over 100 spectra resulted in a range of scattering patterns characteristic of lamellar phases of various dimensions and a coexisting micellar phase. Individual lamellar spectra exhibited single or double peaks or, indeed, broad features comprising several peaks. Moreover, all lamellar spectra included a micellar component with different relative proportions that could be resolved experimentally. The distribution of lamellar spacings was found to be relatively small, between 37.5 and 39.5 Å, effectively continuous, and nearly symmetrical with an average d = 38.2 Å. No statistical correlation was found between lamellar d spacings and the occurrence of coexisting peaks, suggesting that this distribution is intrinsic to the isomeric complexity of NaLAS. The scattering from the coexisting micellar phase could be deconvoluted from the overall signal, and its SAXS pattern could be well described by polydisperse (≈20%) core−shell spheres of 32 Å diameter, interacting via a standard screened electrostatic repulsion potential. On average, the fraction of micellar to lamellar phases is found to be 39 vol %. Within the micellar phase, the concentration of micelles is approximately 17 vol %.

The 45% NaLAS aqueous solution is evidently spatially heterogeneous. From the illuminated scattering volume and flow rate, one can estimate a characteristic length scale for such heterogeneity to be of the order of 50 nL, corresponding to a linear dimension of approximately 350 μm. Large spatial variations can be qualitatively confirmed by polarized light optical microscopy.

As expected, MLV and lamellar phases are found to respond differently under flow. The MLV phase, prepared under shear at 33% mass fraction and addition of sodium sulfate, is found to be comparatively impervious to contraction−expansion flow. Its scattering pattern was found to remain isotropic and the lamellar spacing unchanged under all conditions investigated. By contrast, the lamellar phase counterpart exhibited strong alignment even under gentle extensional fields. Prior to entering a constriction, isotropic scattering patterns are broadly observed. Lamellar sheets then orient along the direction of the flow within the constriction and then normal to this direction upon exiting, thereby undergoing an orientational flip. The degree of lamellar sheet alignment and orientation is discussed in terms of a director characterizing the structure under flow and compared with the experimentally measured flow field by optical microscopy. The bilayer director and flow velocity at the exit of a constriction are found to be remarkably well correlated (except near channel walls where the fluid experiences additional shear).

Our results demonstrate that despite the compositional complexity inherent to NaLAS, the structure and flow response of liquid crystalline solutions can be rigorously elucidated by microfluidic SAXS, providing unique insight into this important surfactant system of academic and industrial relevance.

AUTHOR INFORMATION

Corresponding Authors

*E-mail a.poulos@imperial.ac.uk (A.S.P.).
*E-mail j.cabral@imperial.ac.uk (J.T.C.).

Notes

The authors declare no competing financial interest.

ACKNOWLEDGMENTS

We thank Procter & Gamble for financial support and the Engineering and Physical Sciences Research Council (EPSRC) for a knowledge transfer secondment for A.S.P. and financial support through grants EP/L020564/1 and EP/L022176/1. We thank the Institute of Chemical Biology, EPSRC, and Procter & Gamble for a PhD studentship for R.M.M. We thank Carlos Gonzalez Lopez for assistance with the preparation of the microfluidic devices and Alisyn Nedoma for advice on SAXS data reduction. Diamond Light Source is acknowledged for beamtime. Data is available on request: please contact polymer-microfluidics@imperial.ac.uk.

REFERENCES

(1) Stewart, J. A.; Saiani, A.; Bayly, A.; Tiddy, G. J. T. The Phase Behaviour of Lyotropic Liquid Crystals in Linear Alkylbenzene Sulphonate (LAS) Systems. *Colloids Surf., A* **2009**, *338*, 155−161.
(2) Cates, M. E.; Evans, M. R. *Soft and Fragile Matter: Nonequilibrium Dynamics, Metastability and Flow (Pbk)*; CRC Press: 2000.
(3) Larson, R. G. *The Structure and Rheology of Complex Fluids*; Oxford University Press: New York, 1999; Vol. *33*.
(4) Silva, B. F. B.; Zepeda-Rosales, M.; Venkateswaran, N.; Fletcher, B. J.; Carter, L. G.; Matsui, T.; Weiss, T. M.; Han, J.; Li, Y. L.; Olsson, U.; Safinya, C. R. Nematic Director Reorientation at Solid and Liquid Interfaces under Flow: SAXS Studies in a Microfluidic Device. *Langmuir* **2015**, *31* (14), 4361−4371.
(5) Lopez, C. G.; Watanabe, T.; Martel, A.; Porcar, L.; Cabral, J. T. Microfluidic-SANS: Flow Processing of Complex Fluids. *Sci. Rep.* **2015**, *5*, 7727.
(6) Eberle, A. P. R.; Porcar, L. Flow-SANS and Rheo-SANS applied to soft matter. *Curr. Opin. Colloid Interface Sci.* **2012**, *17*, 33−43.
(7) Lettinga, M. P.; Holmqvist, P.; Ballesta, P.; Rogers, S.; Kleshchanok, D.; Struth, B. Nonlinear Behavior of Nematic Platelet Dispersions in Shear Flow. *Phys. Rev. Lett.* **2012**, *109*, 246001−246001.
(8) Hargreaves, A. E.; Hargreaves, T. *Chemical Formulation: An Overview of Surfactant-Based Preparations Used in Everyday Life*; Royal Society of Chemistry: 2003; Vol. *32*.
(9) Laughlin, R. G. *The Aqueous Phase Behavior of Surfactants*; Academic Press: London, 1994; Vol. *6*.
(10) Mezzenga, R.; Meyer, C.; Servais, C.; Romoscanu, A. I.; Sagalowicz, L.; Hayward, R. C. Shear Rheology of Lyotropic Liquid Crystals: A Case Study. *Langmuir* **2005**, *21* (8), 3322−3333.

DOI: 10.1021/acs.langmuir.6b01240
Langmuir 2016, 32, 5852−5861

(11) Jones, J. L.; McLeish, T. C. B. Rheological Response of Surfactant Cubic Phases. *Langmuir* **1995**, *11* (3), 785−792.
(12) Montalvo, G.; Valiente, M.; Rodenas, E. Rheological Properties of the L Phase and the Hexagonal, Lamellar, and Cubic Liquid Crystals of the CTAB/Benzyl Alcohol/Water System. *Langmuir* **1996**, *12* (21), 5202−5208.
(13) Safinya, C. R.; Roux, D.; Smith, G. S.; Sinha, S. K.; Dimon, P.; Clark, N. A.; Bellocq, A. M. Steric Interactions in a Model Multimembrane System: A Synchrotron X-Ray Study. *Phys. Rev. Lett.* **1986**, *57* (21), 2718−2721.
(14) Ponsinet, V.; Talmon, Y. Direct Imaging of Lamellar Phases by Cryo-Transmission Electron Microscopy. *Langmuir* **1997**, *13* (26), 7287−7292.
(15) Cui, H.; Hodgdon, T. K.; Kaler, E. W.; Abezgauz, L.; Danino, D.; Lubovsky, M.; Talmon, Y.; Pochan, D. J. Elucidating the Assembled Structure of Amphiphiles in Solution Via Cryogenic Transmission Electron Microscopy. *Soft Matter* **2007**, *3* (8), 945−955.
(16) Diat, O.; Roux, D.; Nallet, F. Effect of Shear on a Lyotropic Lamellar Phase. *J. Phys. II* **1993**, *3* (9), 1427−1452.
(17) Safinya, C. R.; Sirota, E. B.; Bruinsma, R. F.; Jeppesen, C.; Plano, R. J.; Wenzel, L. J. Structure of Membrane Surfactant and Liquid-Crystalline Smectic Lamellar Phases under Flow. *Science* **1993**, *261* (5121), 588−591.
(18) Franco, J. M.; Munoz, J.; Gallegos, C. Transient and Steady Flow of a Lamellar Liquid-Crystalline Surfactant Water-System. *Langmuir* **1995**, *11* (2), 669−673.
(19) Lauger, J.; Linemann, R.; Richtering, W. Shear Orientation of a Lamellar Lyotropic Liquid-Crystal. *Rheol. Acta* **1995**, *34* (2), 132−136.
(20) Weigel, R.; Lauger, J.; Richtering, W.; Lindner, P. Anisotropic Small Angle Light and Neutron Scattering from a Lyotropic Lamellar Phase under Shear. *J. Phys. II* **1996**, *6* (4), 529−542.
(21) Penfold, J.; Staples, E.; Lodhi, A. K.; Tucker, I.; Tiddy, G. J. T. Shear-Induced Transformations in the Lamellar Phase of Hexaethylene Glycol Monohexadecyl Ether. *J. Phys. Chem. B* **1997**, *101* (1), 66−72.
(22) Diat, O.; Roux, D. Preparation of Monodisperse Multilayer Vesicles of Controlled Size and High Encapsulation Ratio. *J. Phys. II* **1993**, *3* (1), 9−14.
(23) Van der Linden, E.; Hogervorst, W. T.; Lekkerkerker, H. N. W. Relation between the Size of Lamellar Droplets in Onion Phases and Their Effective Surface Tension. *Langmuir* **1996**, *12*, 3127−3130.
(24) Pommella, A.; Caserta, S.; Guida, V.; Guido, S. Shear-Induced Deformation of Surfactant Multilamellar Vesicles. *Phys. Rev. Lett.* **2012**, *108*, 13.
(25) Pommella, A.; Caserta, S.; Guido, S. Dynamic Flow Behaviour of Surfactant Vesicles under Shear Flow: Role of a Multilamellar Microstructure. *Soft Matter* **2013**, *9* (31), 7545−7552.
(26) Gentile, L.; Behrens, M. A.; Porcar, L.; Butler, P.; Wagner, N. J.; Olsson, U. Multilamellar Vesicle Formation from a Planar Lamellar Phase under Shear Flow. *Langmuir* **2014**, *30* (28), 8316−25.
(27) de Silva, J.; Poulos, A.; Pansu, B.; Davidson, P.; Kasmi, B.; Petermann, D.; Asnacios, S.; Meneau, F.; Impéror, M. Rheological Behaviour of Polyoxometalate-Doped Lyotropic Lamellar Phases. *Eur. Phys. J. E: Soft Matter Biol. Phys.* **2011**, *34* (1), 1−9.
(28) Gentile, L.; Behrens, M. A.; Balog, S.; Mortensen, K.; Ranieri, G. A.; Olsson, U. Dynamic Phase Diagram of a Nonionic Surfactant Lamellar Phase. *J. Phys. Chem. B* **2014**, *118* (13), 3622−9.
(29) Sato, D.; Obara, K.; Kawabata, Y.; Iwahashi, M.; Kato, T. Re-Entrant Lamellar/Onion Transition with Varying Temperature under Shear Flow. *Langmuir* **2013**, *29* (1), 121−132.
(30) Oliviero, C.; Coppola, L.; Gianferri, R.; Nicotera, I.; Olsson, U. Dynamic Phase Diagram and Onion Formation in the System C10E3/D2O. *Colloids Surf., A* **2003**, *228* (1−3), 85−90.
(31) Brooks, M. S.; Moggridge, G. D. The Effect of Additives and the Stability of Multilamellar Vesicles in a Commercial Surfactant System. *Chem. Eng. Res. Des.* **2006**, *84* (2), 139−146.
(32) Hart, A. Effect of Particle Size on Detergent Powders Flowability and Tabletability. *J. Chem. Eng. Process Technol.* **2015**, *6*, 215.
(33) Ma, J.-G.; Boyd, B. J.; Drummond, C. J. Positional Isomers of Linear Sodium Dodecyl Benzene Sulfonate: Solubility, Self-Assembly, and Air/Water Interfacial Activity. *Langmuir* **2006**, *22* (21), 8646−8654.
(34) Ockelford, J.; Timimi, B. A.; Narayan, K. S.; Tiddy, G. J. T. An Upper Critical-Point in a Lamellar Liquid-Crystalline Phase. *J. Phys. Chem.* **1993**, *97* (26), 6767−6769.
(35) Richards, C.; Tiddy, G. J. T.; Casey, S. Lateral Phase Separation Gives Multiple Lamellar Phases in a "Binary" Surfactant/Water System: The Phase Behavior of Sodium Alkyl Benzene Sulfonate/Water Mixtures. *Langmuir* **2007**, *23* (2), 467−474.
(36) Stewart, J. A.; Saiani, A.; Bayly, A.; Tiddy, G. J. T. Phase Behavior of Lyotropic Liquid Crystals in Linear Alkylbenzene Sulphonate (LAS) Systems in the Presence of Dilute and Concentrated Electrolyte. *J. Dispersion Sci. Technol.* **2011**, *32* (12), 1700−1710.
(37) Pike, L. J. Lipid Rafts: Bringing Order to Chaos. *J. Lipid Res.* **2003**, *44* (4), 655−667.
(38) Gevgilili, H.; Kalyon, D.; Birinci, E.; Malik, M.; Goovaerts, L.; Bacon, R.; Mort, P. Dynamic Assembly of Anionic Surfactant into Highly-Ordered Vesicles. *J. Colloid Interface Sci.* **2011**, *356* (2), 579−588.
(39) Martin, H. P.; Brooks, N. J.; Seddon, J. M.; Luckham, P. F.; Terrill, N. J.; Kowalski, A. J.; Cabral, J. T. Microfluidic Processing of Concentrated Surfactant Mixtures: Online SAXS, Microscopy and Rheology. *Soft Matter* **2016**, *12*, 1750−1758.
(40) Martin, H. P.; Brooks, N. J.; Seddon, J. M.; Terrill, N. J.; Luckham, P. F.; Kowalski, A. J.; Tcabral, J. Complex Fluids Under Microflow Probed By SAXS Rapid Microfabrication And Analysis. *J. Phys.: Conf. Ser.* **2010**, *247* (1), 012050−012050.
(41) Ilavsky, J. Nika: Software for Two-Dimensional Data Reduction. *J. Appl. Crystallogr.* **2012**, *45*, 324−328.
(42) Dierking, I. *Textures of Liquid Crystals*; John Wiley & Sons: 2006.
(43) Paasch, S.; Schambil, F.; Schwuger, M. J. Rheological Properties of Lamellar Lyotropic Liquid Crystals. *Langmuir* **1989**, *5* (6), 1344−1346.
(44) Nallet, F.; Laversanne, R.; Roux, D. Modelling X-Ray or Neutron Scattering Spectra of Lyotropic Lamellar Phases: Interplay between Form and Structure Factors. *J. Phys. II* **1993**, *3* (4), 487−502.
(45) Hansen, J.-P.; Hayter, J. B. A rescaled MSA structure factor for dilute charged colloidal dispersions. *Mol. Phys.* **1982**, *46* (3), 651−656.
(46) Hayter, J. B.; Penfold, J. An analytic structure factor for macroion solutions. *Mol. Phys.* **1981**, *42* (1), 109−118.
(47) Trebbin, M.; Steinhauser, D.; Perlich, J.; Buffet, A.; Roth, S. V.; Zimmermann, W.; Thiele, J.; Forster, S. Anisotropic Particles Align Perpendicular to the Flow Direction in Narrow Microchannels. *Proc. Natl. Acad. Sci. U. S. A.* **2013**, *110* (17), 6706−6711.
(48) Idziak, S. H. J.; Welch, S. E.; Kisilak, M.; Mugford, C.; Potvin, G.; Veldhuis, L.; Sirota, E. B. Undulating Membrane Structure under Mixed Extensional-Shear Flow. *Eur. Phys. J. E: Soft Matter Biol. Phys.* **2001**, *6* (2), 139−145.
(49) Penfold, J.; Staples, E.; Tucker, I.; Carroll, P.; Clayton, I.; Cowan, J. S.; Lawton, G.; Amin, S.; Ferrante, A. Ruddock, N. Elongational Flow Induced Ordering in Surfactant Micelles and Mesophases. *J. Phys. Chem. B* **2006**, *110* (2), 1073−1082.
(50) Roux, D.; Nallet, F.; Freyssingeas, E.; Porte, G.; Bassereau, P.; Skouri, M.; Marignan, J. Excess Area in Fluctuating-Membrane Systems. *Europhys. Lett.* **1992**, *17* (7), 575−581.

DOI: 10.1021/acs.langmuir.6b01240
Langmuir 2016, 32, 5852−5861